Research Article

Ghada ALMisned, Ziad Y. Khattari, Elaf Rabaa, Yasser S. Rammah, Duygu Sen Baykal, Gokhan Kilic, Hesham M. H. Zakaly, Antoaneta Ene*, and Huseyin Ozan Tekin*

Tailoring a symmetry for material properties of tellurite glasses through tungsten(VI) oxide addition: Mechanical properties and gamma-ray transmissions properties

https://doi.org/10.1515/arh-2022-0151
received February 24, 2023; accepted April 19, 2023

Abstract: We report a correlation outcome for mechanical and gamma-ray transmission properties of tellurite glasses by increasing tungsten(VI) oxide concentration in glass structure. The mechanical properties as well as Poisson's ratio (σ) of the studied glasses are estimated by applying Makishima–Mackenzie model. Gamma-ray attenuation properties using various fundamental parameters are determined in 0.015–15 MeV energy range. Poisson's ratio (σ) decreased from 0.43017 to 0.42711, while all elastic moduli increased linearly with the molar increment of either [WO_3] or [TeO_2] in the molecular structure of the glass network. Moreover, gamma-ray attenuation properties are enhanced as a function of increasing WO_3 substitution amount from 30 to 50% mol in the glass structure. Half-value layer values at 15 MeV are found to be between 2.648 and 2.8614 cm. I4 samples with a composition of $20TeO_2$–$50WO_3$–$30GdF_3$ and density of 6.0530 g/cm^3 was found to have superior material properties in terms of elastic and gamma-ray attenuation properties. It can be concluded that maximized WO_3 contribution into the tellurite glasses may be considered as a critical tool in terms of establishing a symmetry between mechanical and gamma-ray attenuation properties for high-density tellurite glasses for their potential utilization in nuclear waste management, radiation shielding, and radioactive source transportation purposes.

Keywords: tellurite glasses, tungsten(VI) oxide, mechanical properties, shielding

*** Corresponding author: Antoaneta Ene,** INPOLDE Research Center, Department of Chemistry, Physics and Environment, Faculty of Sciences and Environment, Dunarea de Jos University of Galati, 47 Domneasca Street, 800008 Galati, Romania, e-mail: Antoaneta.Ene@ugal.ro
*** Corresponding author: Huseyin Ozan Tekin,** Medical Diagnostic Imaging Department, College of Health Sciences, University of Sharjah, Sharjah, 27272, United Arab Emirates; Computer Engineering Department, Faculty of Engineering and Natural Sciences, Istinye University, Istanbul 34396, Turkey, e-mail: tekin765@gmail.com
Ghada ALMisned: Department of Physics, College of Science, Princess Nourah Bint Abdulrahman University, P.O. Box 84428, Riyadh 11671, Saudi Arabia
Ziad Y. Khattari: Department of Physics, Faculty of Science, The Hashemite University, P.O. Box 330127, Zarqa 13133, Jordan
Elaf Rabaa: Medical Diagnostic Imaging Department, College of Health Sciences, University of Sharjah, Sharjah, 27272, United Arab Emirates
Yasser S. Rammah: Department of Physics, Faculty of Science, Menoufia University, Shebin El-Koom 32511, Menoufia, Egypt
Duygu Sen Baykal: Istanbul Kent University, Vocational School of Health Sciences, Medical Imaging Techniques, Istanbul 34433, Turkey
Gokhan Kilic: Department of Physics, Faculty of Science, Eskisehir Osmangazi University, Eskisehir, 26040, Turkey
Hesham M. H. Zakaly: Institute of Physics and Technology, Ural Federal University, 620002 Ekaterinburg, Russia; Physics Department, Faculty of Science, Al-Azhar University, Assiut 71524, Egypt

1 Introduction

Using radiation in medical and industrial applications has resulted in significant benefits for scientific society. Ionizing radiation, which can be used for medical purposes, has risen to an indispensable position in medical applications because of its revolutionary contributions to the diagnosis and treatment of various diseases. Nevertheless, the presence of these benefits does not indicate that the detrimental biological consequences resulting from the radiation's ionizing qualities be ignored. In situations other than the intended use of ionizing radiation, the exposure should be reduced, and the essential application procedures should be carried out with the lowest possible dose exposure to the patients. In terms of the importance

of separating the operating room from the device room and providing radiation shielding, the diagnostic radiology facilities may be seen as an important area in terms of underlining the importance of transparent shielding materials. In general, separating the device operating room from the device room with a glass absorber minimizes the workers from being exposed in the control room to X-rays [1]. Transparency of the glass material to be utilized is crucial under these circumstances to ensure that patient monitoring is maximally maintained [1,2]. In addition, several application areas, such as the transportation and storage of resources in nuclear medicine fields and the protection of waste resources, may be cited as significant aspects of medical radiation fields. Lead (Pb) and concrete are two major shielding materials for X-rays and gamma-rays, according to their traditional applications [3–6]. The toxicity and lack of transparency, along with the disadvantaged material properties, put glass-based materials in the spotlight as alternative radiation shielding materials after showing great potential properties [7–12]. Despite the high density of lead and its success in attenuating photon energies, the fact that it is toxic, heavy, and opaque material has made it difficult to manufacture materials for eye shielding, viewing box, and full body aprons. On the other hand, concrete has proven its high durability and high absorbing factor against X-ray and gamma rays, yet the disadvantage of the possibility that it would fracture and lose its moisture content made it challenging to ensure high protection [13,14]. Furthermore, glass has been a potential option to replace concrete, for its properties of being transparent, easy to fabricate, high homogeneity, and ability to accommodate a wide variety of heavy metal components [15–17] in their matrix, shielding material properties can be improved and maintained. Among different glasses, tellurium (TeO_2) glass type made an obvious place as a material in lasers, fibers, and non-linear optical devices in recent years [18–21], due to its high density, high dielectric constant feature, low melting point, and infrared transmittance ability [22]. TeO_2 glass-forming oxide was selected in this study due to its non-crystalline nature, low transition temperature, and high chemical stability [23], along with WO_3 as a second glass-forming oxide, since TeO_2 requires secondary component to form glass. Moreover, WO_3 is known widely in electrochromic, photochromic, and gas sensing materials, along with other applications due to its special physical and chemical properties [24], which may provide a good option to improve the glass system, by ensuring anti-crystallization, maintaining a high density and index of refraction, and increasing the glass transition temperature. Comprehensive structural study of tungsten oxide–tellurite binary glasses (TeO_2–WO_3) is found in the literature as one of the main studies on this subject [25]. Radiation shielding properties of binary TeO_2–WO_3 glasses were studied by Sayyed et al. [26]. In a study carried out on the structural and physical properties of TeO_2–WO_3 glasses containing Li_2O, an alkali oxide [27], since the densities of the synthesized samples are lower than the metal oxide doped TeO_2–WO_3 glasses, we can say that this is not advantageous with respect to radiation shielding studies. Although PbO-doped tungsten oxide–tellurite glasses [28] have the highest density among these glass groups, it can be said that the density values are close when compared to the gadolinium fluoride (GdF_3)-doped glasses discussed in this study and is more advantageous considering the harmful effect of PbO to nature. The last component in this study is GdF_3 [29], since it has been a good host of fluorescent materials, and exhibits evidence of its potential properties including high density, high transmission, and maintain glass stability. Unlike our previous studies [30–32], in which we examined the radiation properties of similar compositions including TeO_2, WO_3, and GdF_3, in this study four glass samples with higher WO_3 (i.e., from 30 to 50 mol%) concentration and gradually decreasing TeO_2 concentration (i.e., from 40 to 20 mol%) were examined. In an effort to accomplish this, we have selected four distinct composition samples of glass materials and analyzed their crucial elastic moduli, mechanical properties, and gamma-ray shielding properties using theoretical approaches. The main purpose of this study is to determine the effect of high mole ratio WO_3 on the mechanical properties and gamma-ray attenuation coefficient in tellurite glasses and to demonstrate its suitability for radiation shielding applications.

2 Materials and methods

The absorber material's gamma-ray attenuation properties are determined by dividing the incoming gamma-ray intensity by the secondary gamma-ray intensity, which is lowered by the material. The attenuation coefficient of the substance may be calculated using this configuration. One example of a transmission assembly is seen in Figure 1. In this stage of the previous study, we have acquired essential data on the gamma-ray absorption capabilities of TeO_2–WO_3–GdF_3 [29] glass samples and investigated it. Four glass samples with different compositions were considered to determine their numerous gamma-ray shielding properties and mechanical properties. Using Py-MLBUF software [33], gamma-ray shielding parameters have been concluded in the range of 0.015–15 MeV. Next, we demonstrated

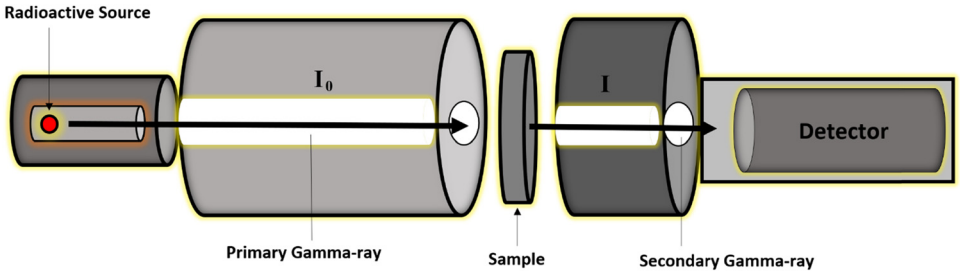

Figure 1: Transmission setup for gamma-rays.

the findings through ORIGIN2018 software. Using a variety of crucial parameters such as mass attenuation coefficient, linear attenuation coefficient (μ), half-value layer (HVL) for each glass sample as a function of energy, a monotonic impact of increasing WO_3 amount from 30 to 50% mol against decreasing TeO_2 amount was investigated. Moreover, additional calculations for evaluating the efficiency of glass samples were performed using mean free path (mfp), effective electron conductivity (C_{eff}), effective electron density (N_{eff}), and effective atomic number (Z_{eff}) over a range of photon energy between 0.0.15 and 15 MeV. Overall, through our previous investigations and other published studies, one may attain more detailed technical information, as well as theoretical calculations related to these important factors for gamma-ray attenuation properties.

3 Results and discussion

3.1 Transmission of gamma-ray through the glass samples

In this study, four glass samples encoded as I1, I2, I3, and I4 along with different concentrations of WO_3 were taken separately for critical gamma-ray absorption parameter calculations through Py-MLBUF program. In absorbing gamma rays and X-rays, density (g/cm^3) and the physical characteristics of shielding materials are often correlated. Due to the existence of high electrons in high-density materials, incoming photons are effectively absorbed by strong internal interactions, which are efficient at absorbing this type of radiation. We focused on the glass densities (Table 1) [29], where they revealed having distinct values due to their different chemical compositions. Figure 2 demonstrates the densities of four glass samples, I4 with 20% of TeO_2, 50% of WO_3, and 30% of GdF_3 sample proved to have the highest density among all tested samples (i.e., 6.053 g/cm^3), where an obvious drop of density is seen in I1 sample which contains 40% of TeO_2, 30% of WO_3, and 30% GdF_3. I4's WO_3 composition was the greatest as 50%, while I1's WO_3 composition was the lowest at 30%. The density of the glass samples was therefore increased by the presence of a significant WO_3 component. In addition, coefficients of linear attenuation (μ) from 0.015 to 15 MeV have been determined. Figure 3 shows the linear attenuation coefficient (μ) values as a function of increasing energy for the four glass samples. Low energy photons are typically affected by the photoelectric effect owing the predominancy of this effect in aforementioned energy zone [34]. However, when the energy increases, a clear fall in (μ) values is seen owing to the predominating Compton scattering effect. The graph demonstrates a decline from 0.04 followed by unstable high and low values of the four samples around the k-absorption edge point, where a steady decline started from 0.06 keV affecting Compton effect [34]. I4 sample with the maximum WO_3 contribution in glass configuration reported to have the highest value of linear attenuation coefficient among almost all energy levels. The results obtained indicate that the increase in WO_3-doping in the tellurite glass system leads to improvements in both density and linear attenuation coefficient values. Another essential gamma-ray absorbing parameter, mass attenuation coefficient (μ_m), which represents the normalization of the materials density, would be rather calculated by per unit mass that consider a crucial data in determining the absorber performance. Figure 4 represents the variation of μ_m values in the

Table 1: Sample codes, molar compositions of compounds and densities [29]

Sample code	TeO_2 (mol%)	WO_3 (mol%)	GdF_3 (mol%)	Density (g/cm^3)
I1	40	30	30	5.8314
I2	30	50	20	5.9453
I3	30	40	30	5.9937
I4	20	50	30	6.0530

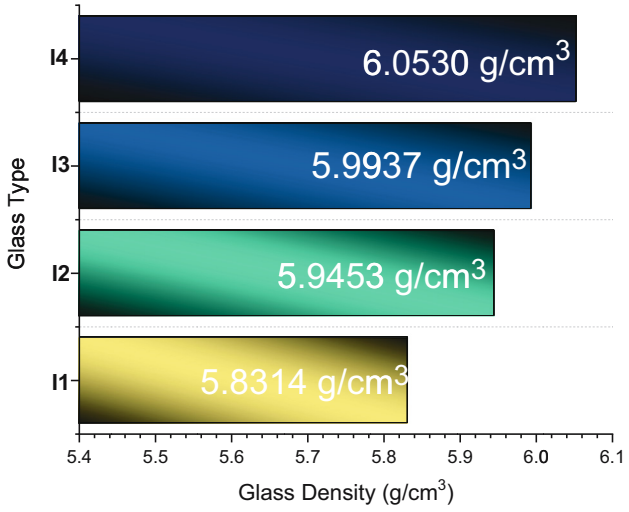

Figure 2: Variation of investigated glass densities.

range of 0.015–15 MeV, where the greatest values of μ_m have been reported in the low energy range and the lowest values have been reported in the high energy range. Among all samples, I4 sample, with the high concentration of 50% WO_3, was observed with the maximum μ_m values, due to the large atomic number of W that enhanced the glass system properties in both linear and mass attenuation coefficients in the used specific energy scale. In addition, HVL investigation has been done which covers a crucial position in shielding investigations as it represents the lowest-possible absorber thickness required to lower the intensity of the primary photons by its half-value. Performance of a material may be assessed through the halving of incident gamma-ray intensity within the lowest material thickness possible. In Figure 5, the variations of HVL levels as a function of increasing energy are seen for the four glass samples. The HVL values increase as the energy of the incoming photon increased, demonstrating different levels of values for material samples. I4 sample had the lowest HVL value among all glass samples tested as the energy increases making it a superior sample among all samples in determining the optimum radiation shielding material. For instance, HVL values reported for the four glass samples I1, I2, I3, and I4 at 15 MeV are 2.8614, 2.7159, 2.728, and 2.648 cm, respectively. I4 glass sample would decrease the initial intensity of an incoming photons to half with the smallest possible thickness due to the highest WO_3 amount in its composition. Another

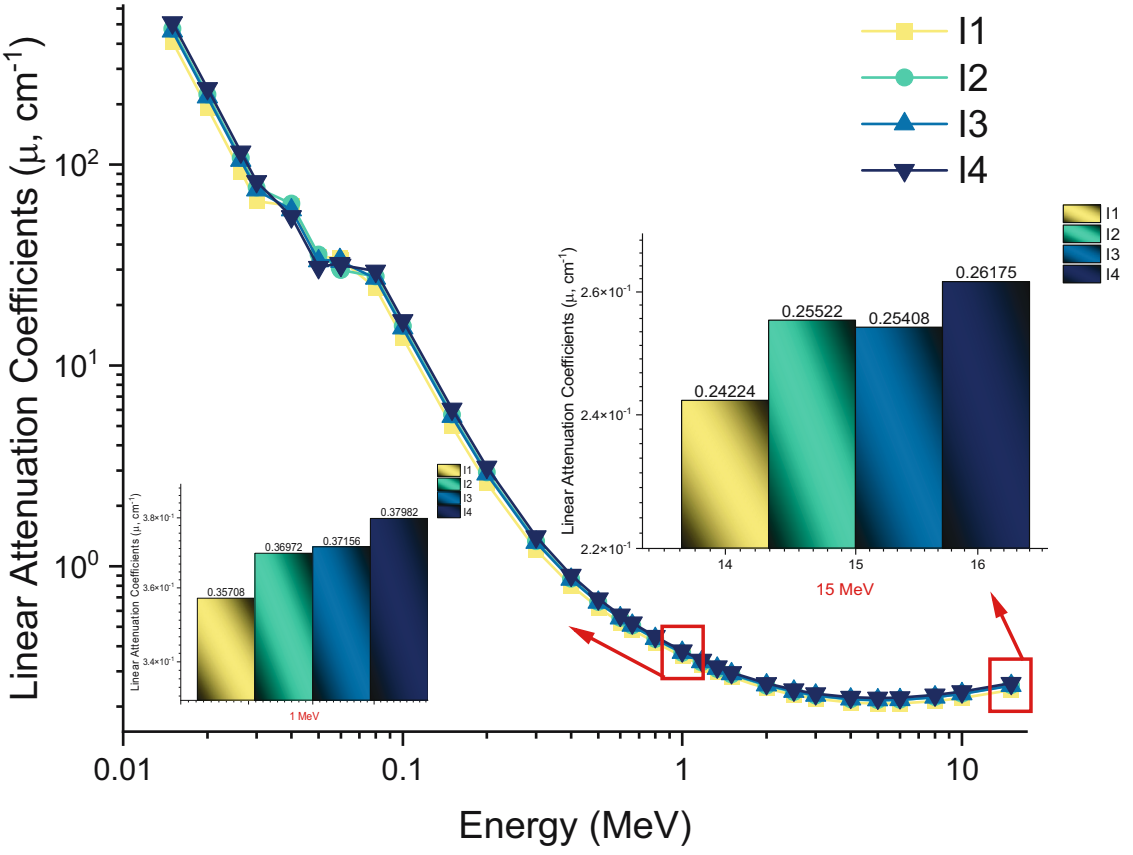

Figure 3: Variation of linear attenuation coefficient (cm^{-1}) with photon energy (MeV) for all I1–I4 glasses.

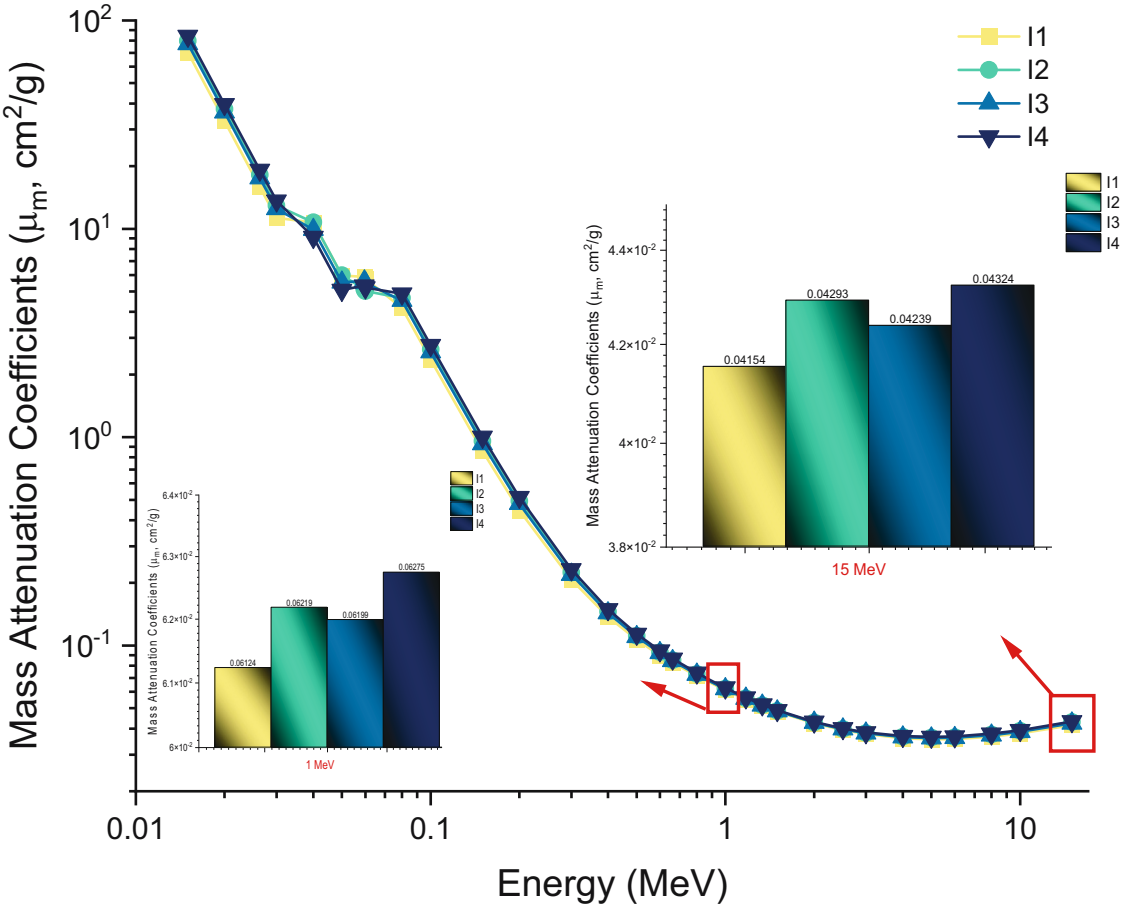

Figure 4: Variation of mass attenuation coefficients (cm^2/g) with photon energy (MeV) for all I1–I4 glasses.

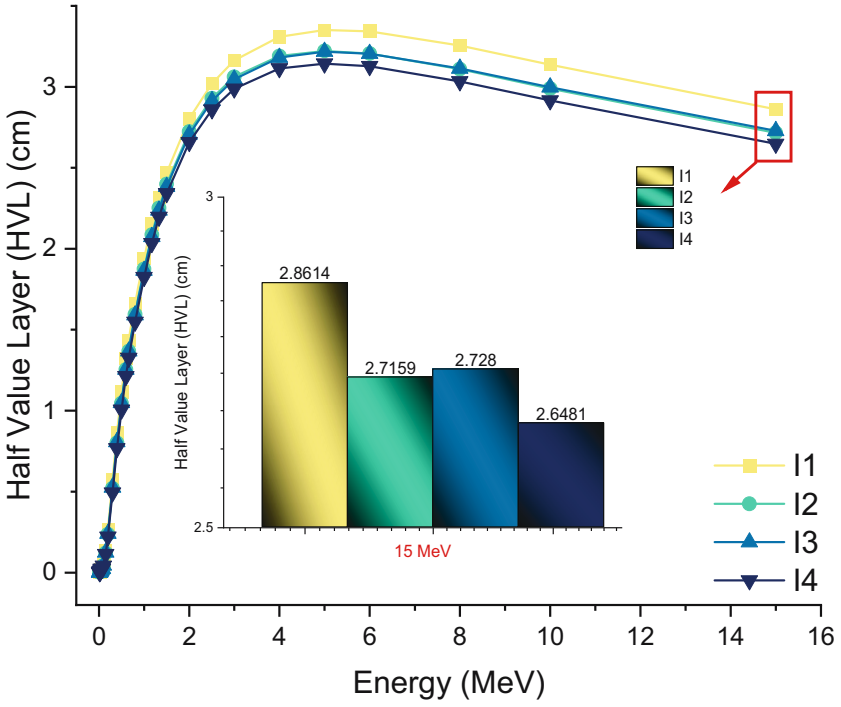

Figure 5: Variation of HVL (cm) with photon energy (MeV) for all I1–I4 glasses.

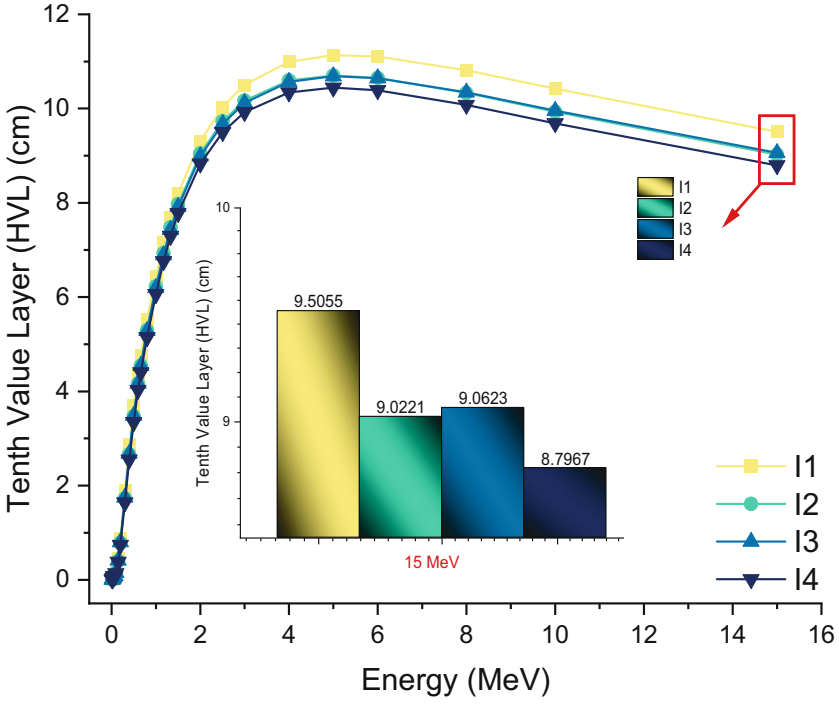

Figure 6: Variation of tenth value layer (cm) with photon energy (MeV) for all I1–I4 glasses.

fundamental attenuation indicator is the mfp, which indicates the average path of a moving gamma-ray between interactions that might alter its direction or energy that also demonstrates the attenuation radiation ability in a material (Figure 6). Figure 7 indicates the relationship of the mfp values (cm) with respect to increasing the incoming photon energy. I4 has been proven to have the lowest mfp among all energy levels due to the superior effect of high

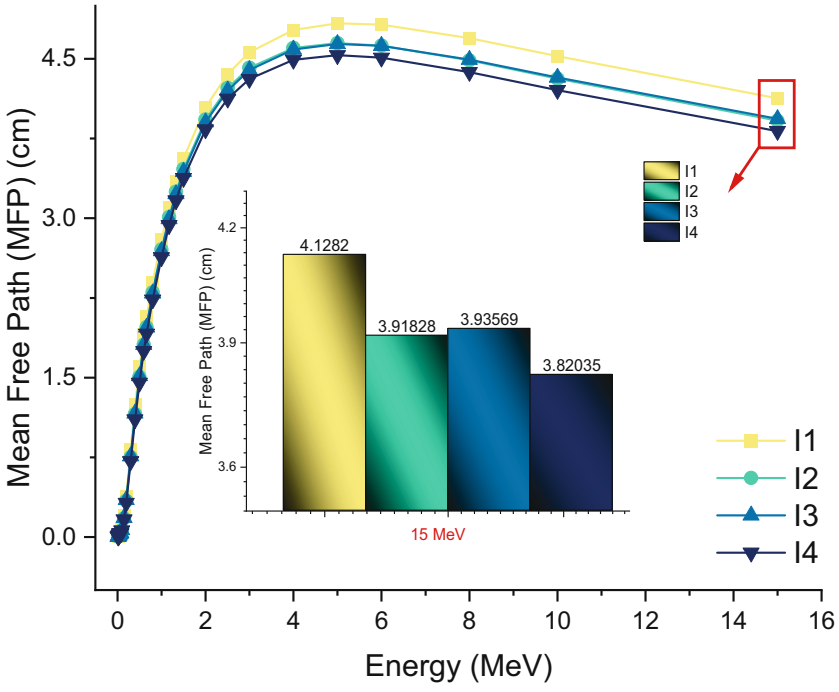

Figure 7: Variation of mfp (cm) with photon energy (MeV) for all I1–I4 glasses.

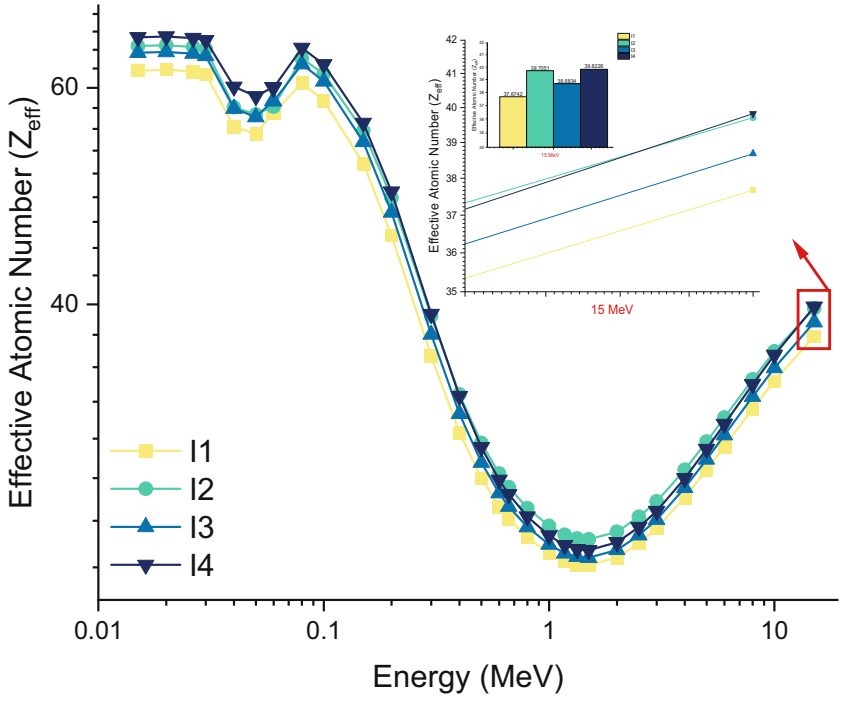

Figure 8: Variation of effective atomic number (Z_{eff}) with photon energy (MeV) for all I1–I4 glasses.

WO_3 composition in gamma-ray absorption property, while lower mfp values indicate the efficiency of the absorber. Meanwhile, the term effective atomic number (Z_{eff}) is another important parameter to be considered in terms of determining the attenuation properties of absorber materials. It is widely recognized that the effective atomic number demonstrates the quantity of electrons in the nucleus orbit, with the Z number indicating the number of electrons present. Thus, the atoms with the higher number of Z values would result in having a high number of electrons, and that the incoming photons may have a high possibility to collide with electrons and reduce its energy. The greater the collision, the greater the possibility that the incoming photon energy would be absorbed through an excitation or through the electron falling out of orbit. Figure 8 displays the variation values of the effective atomic number at 0.015–15 MeV energy levels for I1, I2, I3, and I4 glass samples. In the low energy level range of 0.015–0.3 MeV, the I4 sample exhibits the highest effective atomic number. While, after increasing the energy level of the incoming photon from 0.4 to 15 MeV, I2 sample containing 30% TeO_2, 50% WO_3, and 20% GdF_3 exhibited the greatest effective atomic number. Both samples have the greatest concentration of WO_3, making their gamma-ray absorption characteristics more effective.

3.2 Elastic-mechanical properties

As described in several reports the high atomic packing for glasses is $V_t > 0.60$ [35] and this value agrees with good elastic moduli observed for these glasses [36,37]. Using the theoretical methods of Makishima–Mackenzie [38], Young's (E), shear (S), bulk (B), longitudinal (L) elastic moduli, and micro-hardness (H) of the studied glasses were calculated at various molar fractions of GdF_3, WO_3, and TeO_2 (Table 2). We referred to the published

Table 2: The mechanical parameters and elastic moduli of the investigated samples

Sample code	ΣV_i (cm^3/mol)	G (kJ/cm^3)	V_t (cm^3/mol)	E (GPa)	B (GPa)	S (GPa)	L (GPa)	σ	H (GPa)
I1	17.043	48.18	0.50278777	48.449	29.231	19.795	44.077	0.43017	0.01628
I2	18.242	54.26	0.52482053	56.954	35.868	23.051	53.157	0.42711	0.01703
I3	17.703	49.56	0.517867896	51.331	31.899	20.836	47.526	0.42807	0.01679
I4	18.363	50.94	0.524014044	53.387	33.570	21.615	49.781	0.42722	0.01700

relations [38] to ascertain the mechanical parameters. The estimated Poisson's ratio and the anticipated elastic moduli are presented in Table 2. By incorporating the calculated numbers for the abovementioned parameters, we explain and represent the assessed outcomes for other elastic-mechanical parameters as follows. Researchers in material physics frequently assess the various glasses' strengths, including those of glass–ceramic, inorganic, organic, and metallic glasses, utilizing this important physical characteristic [35,39]. It establishes a connection between the mechanical properties of the glass and its chemical composition, metallic transition temperature, and atomic structures depicted in the glassy structure [35]. Moreover, this ratio does not directly take into account the interatomic bonds between the chemical components of glass, instead, it depends on the atomic packing, cross-linking, coordination number, and molecular organization of the glass system under study [40]. In the current work, the results demonstrate that Poisson's glasses ratio changes from 0.430 to 0.427 depending on the molar percentage of GdF_3, WO_3, or TeO_2 present in the glasses. Table 2 also shows the Gibbs free energy-encoded thermodynamic characteristics of the glassy network (G). This metric's range of values is 48.18–50.94 kJ/cm^3. A higher sample density also corresponds with its progressive linear expansion. Also, as shown in Table 2, the molar fractions of WO_3 or TeO_2 in the molecular form of the glassy structure rose linearly with increasing micro-hardness (H) and other moduli. For instance, depending on the molecular makeup of the substance, Young's modulus of a given glass sample may range from 48.45 to 53.45.59 GPa. The interatomic-bonding strength, directional order parameter in the unit cell, and coordination number were responsible for these glasses' elastic properties [41].

4 Conclusion

In recent years, glass has been considered a potential replacement for lead and concrete due to its transparency, ease of fabrication, high homogeneity, and capacity to accommodate a wide range of heavy metal components within its matrix, allowing for improved and maintained shielding material properties. Using the melt quenching method, various quantities of tellurite oxide, tungsten(IV) oxide, and GdF_3 compounds have been previously synthesized. The gamma-ray absorption capabilities of I1, I2, I3, and I4 glass samples were determined by performing fundamental calculations on each sample. Distinct densities have been conducted for the four samples due to their different composition rates, where I4 with 40% of TeO_2, 50% of WO_3, and 30% of GdF_3 was reported with the highest density value (i.e., 6.053 g/cm^3). In the framework of the results obtained from the study, the following propositions were made:

- The high WO_3 concentration has greatly contributed to the I4 sample's high density. In addition, it has high linear and mass attenuation coefficient of 0.37982 and 0.062749 at 1 MeV.
- When comparing the HVL values of the four samples, I4 had the lowest HVL value at the greatest energy of 15 MeV, with a value of 2.648 cm, compared to 2.8614, 2.7159, and 2.728 cm for the other samples I1, I2, and I3.
- The mean free calculation reported I4 along with the lowest value among all the samples, due to the positive influence of WO_3 on the tellurite glass system.

During the investigation of Z_{eff}, two glasses containing the highest composition of WO_3 displayed interesting outcomes. I4 with 20% of TeO_2, 50% of WO_3, and 30% of GdF_3 exhibited the highest effective atomic number in the low energy ranges of 0.015–0.3 MeV, while I2 with 30% TeO_2, 50% WO_3, and 20% GdF_3 exhibited the greatest effective atomic number in the high energy ranges from 0.4 to 15 MeV. In the meantime, the results demonstrated that σ decreased while elastic moduli and micro-hardness parameters increased linearly with the molar increase of either WO_3 or TeO_2 in the glassy network's molecular structure. In conclusion, it is evident from our critical examinations that increasing the quantity of WO_3 in the tellurite glass system has improved its gamma-ray absorption capabilities as well as its mechanical properties, thereby making it a useful instrument in radiation shielding technologies. Future research will determine whether WO_3-containing glasses of varying compositions exhibit comparable effects. Due to its effect on density increase, WO_3 will be considered as a doping agent in the synthesis of prospective radiation-shielding materials.

Acknowledgements: The authors would like to express their deepest gratitude to Princess Nourah bint Abdulrahman University Researchers Supporting Project number (PNURSP2023R149), Princess Nourah bint Abdulrahman University, Riyadh, Saudi Arabia.

Funding information: Princess Nourah bint Abdulrahman University Researchers Supporting Project number (PNURSP2023R149), Princess Nourah bint Abdulrahman University, Riyadh, Saudi Arabia.

Author contributions: H.O.T. – conceptualization, writing – original draft, supervision, writing – review and editing; G.A. – visualization, software, writing – original draft; H.M.H.Z. – formal analysis, data curation; E.R. – data curation, formal analysis, writing – original draft; G.K. – data curation, formal analysis, writing – original draft; Y.S.R. – data curation, formal analysis, writing – original draft; D.S.B. – visualization, software; Z.Y.K. – visualization, software; A.E – methodology, funding acquisition, writing – review and editing (the author A.E. would like to thank Dunarea de Jos University of Galati, Romania, for the material and technical support).

Conflict of interest: None.

Ethical approval: The conducted research is not related to either human or animal use.

Data availability statement: The datasets generated during and/or analyzed during the current study are available from the corresponding author on reasonable request.

References

[1] Tekin HO, Altunsoy EE, Kavaz E, Sayyed MI, Agar O, Kamislioglu M. Photon and neutron shielding performance of boron phosphate glasses for diagnostic radiology facilities. Results Phys. 2019;12:1457–64. doi: 10.1016/j.rinp.2019.01.060.

[2] Akkurt I, Alomari A, Imamoglu MY, Ekmekçi I. Medical radiation shielding in terms of effective atomic numbers and electron densities of some glasses. Radiat Phys Chem. 2023;206:110767. doi: 10.1016/j.radphyschem.2023.110767.

[3] Rezaei-Ochbelagh D, Azimkhani S. Investigation of gamma-ray shielding properties of concrete containing different percentages of lead. Appl Radiat Isotopes. 2012;70(10):2282–6. doi: 10.1016/j.apradiso.2012.06.020.

[4] Akkurt I, Akyildirim H, Mavi B, Kilincarslan S, Basyigit C. Gamma-ray shielding properties of concrete including barite at different energies. Prog Nucl Energy. 2010;52(7):620–3. doi: 10.1016/j.pnucene.2010.04.006.

[5] Kharita MH, Takeyeddin M, Alnassar M, Yousef S. Development of special radiation shielding concretes using natural local materials and evaluation of their shielding characteristics. Prog Nucl Energy. 2008;50(1):33–6. doi: 10.1016/j.pnucene.2007.10.004.

[6] Akkurt I, Basyigit C, Kilincarslan S, Mavi B, Akkurt A. Radiation shielding of concretes containing different aggregates. Cem Concr Compos. 2006;28(2):153–7. doi: 10.1016/j.cemconcomp.2005.09.006.

[7] Naseer KA, Marimuthu K, Al-Buriahi MS, Alalawi A, Tekin HO. Influence of Bi_2O_3 concentration on barium-telluro-borate glasses: physical, structural and radiation-shielding properties. Ceram Int. 2021;47(1):329–40. doi: 10.1016/j.ceramint.2020.08.138.

[8] Rammah YS, El-Agawany FI, Mahmoud KA, El-Mallawany R, Ilik E, Kilic G. FTIR, UV–Vis–NIR spectroscopy, and gamma rays shielding competence of novel ZnO-doped vanadium borophosphate glasses. J Mater Sci: Mater Electron. 2020;31:9099–113. doi: 10.1007/s10854-020-03440-5.

[9] Al-Buriahi MS, Tekin HO, Tonguc BT, Rammah YS, Kavaz E. New transparent rare earth glasses for radiation protection applications. Appl Phys A. 2019;125:866. doi: 10.1007/s00339-019-3077-8.

[10] Singh N, Singh KJ, Singh K, Singh H. Comparative study of lead borate and bismuth lead borate glass systems as gamma-radiation shielding materials. Nucl Instrum Methods Phys Res Sect B: Beam Interact Mater At. 2004;225(3):305–9. doi: 10.1016/j.nimb.2004.05.016.

[11] Halimah MK, Azuraida A, Ishak M, Hasnimulyati L. Influence of bismuth oxide on gamma radiation shielding properties of boro-tellurite glass. J Non-Cryst Solids. 2019;512:140–7. doi: 10.1016/j.jnoncrysol.2019.03.004.

[12] AlBuriahi MS, Hegazy HH, Alresheedi F, Olarinoye IO, Algarni H, Tekin HO, et al. Effect of CdO addition on photon, electron, and neutron attenuation properties of boro-tellurite glasses. Ceram Int. 2021;47:5951–8. doi: 10.1016/j.ceramint.2020.10.168.

[13] Temir A, Zhumadilov K, Zdorovets M, Kozlovskiy A, Trukhanov A. Study of gamma radiation shielding efficiency with radiation-resistant Bi_2O_3–TeO_2–WO_3 ceramics. Solid State Sci. 2021;115:106604. doi: 10.1016/j.solidstatesciences.2021.106604.

[14] Han B, Zhang L, Ou J. Radiation shielding concrete. Smart and multifunctional concrete toward sustainable infrastructures. (Chapter). Singapore: Springer; 2017. doi: 10.1007/978-981-10-4349-9_19.

[15] ALMisned G, Tekin HO, Ene A, Issa SAM, Kilic G, Zakaly HMH. A closer look on nuclear radiation shielding properties of Eu^{3+} doped heavy metal oxide glasses: impact of Al_2O_3/PbO substitution. Materials. 2021;14:5334. doi: 10.3390/ma14185334.

[16] Ersundu AE, Büyükyıldız M, Çelikbilek Ersundu M, Şakar E, Kurudirek M. The heavy metal oxide glasses within the WO_3–MoO_3–TeO_2 system to investigate the shielding properties of radiation applications. Prog Nucl Energy. 2018;104:280–7. doi: 10.1016/j.pnucene.2017.10.008.

[17] Tekin HO, Susoy G, Issa SAM, Ene A, ALMisned G, Rammah YS, et al. Heavy metal oxide (HMO) glasses as an effective member of glass shield family: a comprehensive characterization on gamma ray shielding properties of various structures. J Mater Res Technol. 2022;18:231–44. doi: 10.1016/j.jmrt.2022.02.074.

[18] Kilic G, El Agawany FI, Ilik BO, Mahmoud KA, Ilik E, Rammah YS. Ta_2O_5 reinforced Bi_2O_3–TeO_2–ZnO glasses: fabrication, physical, structural characterization, and radiation shielding efficacy. Opt Mater. 2021;112:110757. doi: 10.1016/j.optmat.2020.110757.

[19] Kilic G, Issever UG, Ilik E. Characterization of Er^{3+} doped ZnTeTa semiconducting oxide glass. J Mater Sci Mater Electron. 2019;30:8920–30. doi: 10.1007/s10854-019-01220-4.

[20] Sayyed MI, Dwaikat N, Mhareb MHA, D'Souza AN, Almousa N, Alajerami YSM, et al. Effect of TeO_2 addition on the gamma

radiation shielding competence and mechanical properties of boro-tellurite glass: an experimental approach. J Mater Res Technol. 2022;18:1017–27. doi: 10.1016/j.jmrt.2022.02.130.
[21] Sayyed MI, Kurtulus R, Balderas CV, Kavas T, Almuqrin AH. X-ray shielding behavior of TeO_2–Li_2O–GeO_2–ZnO–Bi_2O_3 glass system using EPICS2017 library and Phy-X software. Appl Phys A. 2021;127:757. doi: 10.1007/s00339-021-04893-z.
[22] ALMisned G, Tekin HO, Issa SAM, Ersundu MÇ, Ersundu AE, Kilic G, et al. Novel HMO-glasses with Sb_2O_3 and TeO_2 for nuclear radiation shielding purposes: a comparative analysis with traditional and novel shields. Materials. 2021;14:4330. doi: 10.3390/ma14154330.
[23] Al-Mukadam R, Zandona A, Deubener J. Kinetic fragility of pure TeO_2 glass. J Non-Cryst Solids. 2021;554:120595. doi: 10.1016/j.jnoncrysol.2020.120595.
[24] Alharbiy N, Khattari ZY, Rammah YS, Saleh A. Role of Al_2O_3, WO_3, Nb_2O_5, and PbO on the physical, elasto-mechanical and radiation attenuation performance of borotellurite glasses. J Mater Sci Mater Electron. 2023;34:191. doi: 10.1007/s10854-022-09604-9.
[25] Charton P, Gengembre L, Armand P. TeO_2–WO_3 glasses: infrared, XPS and XANES structural characterizations. J Solid State Chem. 2002;168(1):175–83. doi: 10.1006/jssc.2002.9707.
[26] Sayyed MI, Qashou SI, Khattari ZY. Radiation shielding competence of newly developed TeO_2—WO_3 glasses. J Alloy Compd. 2017;696:632–8. doi: 10.1016/j.jallcom.2016.11.160.
[27] Çelikbilek M, Ersundu AE, Aydin S. Preparation and characterization of TeO_2–WO_3–Li_2O glasses. J Non-Cryst Solids. 2013;378:247–53. doi: 10.1016/j.jnoncrysol.2013.07.020.
[28] Munoz-Martín D, Villegas MA, Gonzalo J, Fernández-Navarro JM. Characterisation of glasses in the TeO_2–WO_3–PbO system. J Eur Ceram Soc. 2009;29(14):2903–13. doi: 10.1016/j.jeurceramsoc.2009.04.018.
[29] Li C, Zhang X, Onah VC, Yang W, Leng Z, Han K, et al. Physical and optical properties of TeO_2–WO_3–GdF_2 tellurite glass system. Ceram Int. 2022;48(9):12497–505. doi: 10.1016/j.ceramint.2022.01.116.
[30] ALMisned G, Rabaa E, Rammah YS, Khattari ZY, Baykal DS, Ilik E, et al. A promising glass type in electronic and laser applications: elastic moduli, mechanical, and photon transmission properties of WO_2 reinforced ternary-tellurite glasses. Symmetry. 2023;15:602. doi: 10.3390/sym15030602.
[31] ALMisned G, Rabaa E, Sen Baykal D, Kavaz E, Ilik E, Kilic G, et al. Mechanical properties, elastic moduli, and gamma ray attenuation competencies of some TeO_2–WO_3–GdF_3 glasses: tailoring WO_3–GdF_3 substitution toward optimum behavioral state range. Open Chem. 2023;21(1):20220290. doi: 10.1515/chem-2022-0290.
[32] ALMisned G, Rabaa E, Sen Baykal D, Ilik E, Kilic G, Zakaly HMH, et al. Translocation of tungsten(vi) oxide/gadolinium(iii) fluoride in tellurite glasses towards improvement of gamma-ray attenuation features in high-density glass shields. Open Chem. 2023;21(1):20220289. doi: 10.1515/chem-2022-0289.
[33] Mann KS, Mann SS. Py-MLBUF: development of an online-platform for gamma-ray shielding calculations and investigations. Ann Nucl Energy. 2021;150:107845. doi: 10.1016/j.anucene.2020.107845.
[34] Ilik E. Effect of heavy rare-earth element oxides on physical, optical and gamma-ray protection abilities of zinc-borate glasses. Appl Phys A. 2022;128:496. doi: 10.1007/s00339-022-05642-6.
[35] Rouxel T. Elastic properties and short- to medium-range order in glasses. J Am Ceram Soc. 2007;90(10):3019–39. doi: 10.1111/j.1551-2916.2007.01945.x.
[36] Wood J. Computational methods in reactor shielding. New York, USA: Pergamon Press, Inc.; 1982.
[37] Khattari ZY, Al-Buriahi MS. Monte Carlo simulations and Phy-X/PSD study of radiation shielding effectiveness and elastic properties of barium zinc aluminoborosilicate glasses. Radiat Phys Chem. 2022;195:110091. doi: 10.1016/j.radphyschem.2022.110091.
[38] Makishima A, Mackenzie JD. Direct calculation of Young's modulus of glass. J Non-Cryst Solids. 1973;12(1):35–45. doi: 10.1016/0022-3093(73)90053-7.
[39] To T, Jensen LR, Smedskjaer MM. On the relation between fracture toughness and crack resistance in oxide glasses. J Non-Cryst Solids. 2020;534:119946. doi: 10.1016/j.jnoncrysol.2020.119946.
[40] Ghosh S, Das Sharma A, Mukhopadhyay AK, Kundu P, Basu RN. Effect of BaO addition on magnesium lanthanum alumino borosilicate-based glass–ceramic sealant for anode-supported solid oxide fuel cell. Int J Hydrog Energy. 2010;35(1):272–83. doi: 10.1016/j.ijhydene.2009.10.006.
[41] Lawrance GA. Introduction to coordination chemistry. United Kingdom: John Wiley & Sons, Ltd; 2009.